Acta Mech 228, 1249–1268 (2017)
DOI 10.1007/s00707-016-1756-5

ORIGINAL PAPER

Lukas Moschen · Christoph Adam

Peak floor acceleration demand prediction based on response spectrum analysis of various sophistication

Received: 30 June 2016 / Revised: 6 October 2016 / Published online: 3 December 2016

Abstract This paper addresses the prediction of the median peak floor total acceleration (PFA) demand in spatial elastic structures subjected to seismic excitation. The prediction is based on various response spectrum methods of different degrees of sophistication. Beginning with a recently presented complete-quadratic-combination (CQC) rule for PFA demands, several approximations and simplifications concerning the correlation between modal contributions, peak factors, and cross-spectral moments are discussed, leading to the proposed modified modal combination rules. On several earthquake-excited multi-story spatial generic frame structures, the accuracy of the considered rules is assessed. The outcomes of response history analysis serves as benchmark solution. The results show that the modified CQC rules are simple in practical application and lead to reliable estimations of the median PFA demand of spatial structures with negligible loss of accuracy if peak factors are considered.

1 Introduction

In the past, various simplified methods and procedures have been proposed to predict reliably the peak response of an earthquake-excited structure, without conducting response history analysis (RHA). RHA not only requires the computationally expensive direct solution of the equations of motion in a time-stepping procedure but also sophisticated modeling of the structure, and a set of ground motion records is in general not readily available for the site of the structure.

Several of these simplified procedures belong to the class of response spectrum methods. The idea of a response spectrum method is to combine in a statistical fashion the peak response of the corresponding modal coordinates. Therefore, the coupled set of equations of motion of the multi-degrees-of-freedom (MDOF) structure is decomposed into modal single-degree-of-freedom (SDOF) oscillators. For each modal oscillator, the peak response is predicted by means of a so-called response spectrum, provided in standards and regulations. A response spectrum represents the peak response of an earthquake-excited SDOF oscillator as a function of natural period and damping coefficient. In the subsequent step, the *uni-modal* peak responses are superposed to the physical *multi-modal* peak response of the structure. Response spectrum methods are, however, not straightforward because the information about the phase shift of the modal peak responses is not available. Also, the correlation between closely spaced modes should be considered to obtain an accurate prediction of the seismic response. Thus, most of the response spectrum methods are based on a statistical superposition of the uni-modal contributions.

L. Moschen · C. Adam (✉)
Unit of Applied Mechanics, University of Innsbruck, Technikerstr. 13, 6020 Innsbruck, Austria
E-mail: christoph.adam@uibk.ac.at
Tel.: +43-(0)512 507 61600

L. Moschen
E-mail: lukas.moschen@uibk.ac.at

Response spectrum methods have their origin in the 1950s when Rosenblueth [19] proposed the square-root-of-sum-of-squares (SRSS) modal combination rule. As its name already implies, the squares of the modal peak response are added and subsequently the square root is taken. In the following decades, more sophisticated methods have been developed, such as the complete-quadratic-combination (CQC) rule [6,7]. CQC methods allow to consider the correlation between modal response quantities [6] and to take truncated modes into account [7]. Consequently, the multi-modal peak response can be estimated more reliably if modes are closely spaced and/or if modes are in the high-frequency domain (i.e., if modal periods are larger than the lower corner frequency of the response spectrum). As a further example, more recently the complete SRSS modal combination rule [10] has been presented.

All of these methods have in common that they have been developed for *relative* response quantities, such as structural displacements relative to the base and internal forces. However, in the last two decades the prediction of the *total* floor acceleration became more and more the focus of attention [23]. The reason is the observation that many moderate earthquake events of the past left the load-bearing structure of a building unimpaired; however, the building content (also referred to as nonstructural component—NSC) was heavily damaged, causing a long downtime of the building [8,23]. Consequently, in many affected buildings economic losses from damage to NSCs exceeded by far losses from structural damage, as discussed by Filiatrault and Sullivan [9]. This contribution [9] summarizes the current knowledge on seismic analysis of NSCs, and it identifies major knowledge gaps needed for implementation of performance-based seismic design of these components, representing the next frontier of earthquake engineering [9].

Assessment of *vibratory* NSCs is often based on the acceleration spectrum of a floor within a supporting structure subject to a ground motion, referred to as floor response spectrum. Various research efforts have been made to provide simplified but accurate means of estimating floor response spectra both for elastic and for inelastic load-bearing structures, such as [1,22,29].

Since the maximum force on a *rigid* NSC is proportional to the peak total acceleration of its attachment point in the building, more recently research has been devoted to the development of response spectrum methods for the prediction of peak floor acceleration (PFA) demands. A first step toward PFA assessment by means of response spectrum methods was delivered Taghavi and Miranda [24,25]. In this *extended* CQC rule, where the original CQC method considering high-frequency modes [7] is specialized for total acceleration demands, the so-called peak factors are explicitly neglected and simplified expressions for the correlation coefficients are provided. Recently, Pozzi and Der Kiureghian [17] proposed a CQC rule including peak factors. However, in their application of this rule to a simple beam structure the peak factors have been omitted. While for the CQC rule presented in [17] the required correlation coefficients must be numerically computed, Moschen [12] and Moschen et al. [13] derived analytical expressions for the underlying cross-spectral moments, which allow a deeper insight into the relationship between the governing dynamic parameters. The latter CQC rule for PFA demands has been extensively validated on various planar and spatial generic frame structures by comparing its outcomes with results of RHA [12,13].

In the present contribution, several simplifications of these CQC methods are introduced, and their accuracy is evaluated. The ultimate goal is to reveal the degree of sophistication of the CQC modal combination rule required to reliably predict the median PFA demand of earthquake-excited structures.

2 A response spectrum method for peak floor total accelerations

Point of departure is the coupled set of equations of motion of an elastic multi-degrees-of-freedom (MDOF) frame structure subjected to uniform base excitation $\ddot{u}_g(t)$ [3],

$$\mathbf{M}\ddot{\mathbf{u}}^{(\mathrm{rel})}(t) + \mathbf{C}\dot{\mathbf{u}}^{(\mathrm{rel})}(t) + \mathbf{K}\mathbf{u}^{(\mathrm{rel})}(t) = -\mathbf{M}\mathbf{e}\ddot{u}_g(t), \tag{1}$$

where $\mathbf{M}$ is the mass matrix, $\mathbf{C}$ the damping matrix, and $\mathbf{K}$ the stiffness matrix. The vector $\mathbf{u}^{(\mathrm{rel})}(t)$ contains the N relative deformations related to the N dynamic degrees of freedom with respect to the displacement of the ground, $u_g(t)$. The spatial distribution of inertia forces due to the base excitation is governed by the quasi-static influence vector $\mathbf{e}$. Equation (1) describes the motion of a planar structure or of a spatial structure subjected to horizontal ground motion in one principal direction. The extension to base excitation of a spatial structure in both horizontal principal directions is straightforward, however, for the sake of clarity not further pursued.

The vector of total accelerations, $\ddot{\mathbf{u}}(t) = \ddot{\mathbf{u}}^{(\mathrm{rel})}(t) + \mathbf{e}\ddot{u}_{\mathrm{g}}(t)$, is expanded into the N mode shapes ϕ_i, $i = 1, \ldots, N$. Then, after some algebra, the solution of Eq. (1) in terms of $\ddot{\mathbf{u}}(t)$ can be approximated by the first few n ($<N$) modal contributions as [13,16,17]

$$\ddot{\mathbf{u}}(t) \approx \sum_{i=1}^{n} \phi_i \Gamma_i \ddot{d}_i(t) + \left(\mathbf{e} - \sum_{i=1}^{n} \phi_i \Gamma_i \right) \ddot{u}_{\mathrm{g}}(t) = \ddot{\mathbf{u}}^{(n)}(t) + \mathbf{r}^{(n)} \ddot{u}_{\mathrm{g}}(t), \tag{2}$$

in which $\Gamma_i = \left(\phi_i^{\mathsf{T}} \mathbf{M} \mathbf{e}\right) / \left(\phi_i^{\mathsf{T}} \mathbf{M} \phi_i\right)$ is the generalized participation factor, and $\ddot{d}_i(t) = \ddot{d}_i^{(\mathrm{rel})}(t) + \ddot{u}_{\mathrm{g}}(t)$ denotes the total acceleration of the ith modal coordinate. The modal coordinate $d_i^{(\mathrm{rel})}(t)$ is governed by the ith modal oscillator equation, $\ddot{d}_i^{(\mathrm{rel})}(t) + 2\zeta_i \omega_i \dot{d}_i^{(\mathrm{rel})}(t) + \omega_i^2 d_i^{(\mathrm{rel})}(t) = -\ddot{u}_{\mathrm{g}}(t)$, where ω_i denotes the corresponding circular natural frequency and ζ_i the modal damping ratio. In Eq. (2) the high-frequency modal contribution to the acceleration (relative to the base) has been neglected, and the high-frequency modal contribution of the ground acceleration is expressed in terms of a residual vector, $\mathbf{r}^{(n)}$, in an effort to increase the accuracy if only a few modal contributions n ($<N$) are considered. Based on Eq. (2), in [23] the CQC rule for the mean PFA demand of the kth degree of freedom, in this paper referred to as CQC-pf rule,

$$E\left[\max\left(|\ddot{U}_k|\right)\right] \equiv m_{\mathrm{PFA}_k} \approx \left[\sum_{i=1}^{n} \sum_{j=1}^{n} \frac{p_k}{p_i} \frac{p_k}{p_j} \phi_{i,k} \Gamma_i S_{a,i} \phi_{j,k} \Gamma_j S_{a,j} \rho_{i,j} + \left(\frac{p_k}{p_{\mathrm{g}}} m_{\mathrm{PGA}} r_k^{(n)} \right)^2 \right.$$
$$\left. + 2 m_{\mathrm{PGA}} r_k^{(n)} \frac{p_k}{p_{\mathrm{g}}} \sum_{i=1}^{n} \frac{p_k}{p_i} \phi_{i,k} \Gamma_i S_{a,i} \rho_{i,g} \right]^{\frac{1}{2}} \tag{3}$$

has been derived in analogy to the original CQC rule [7] applicable to relative peak response quantities, see also [13,17]. In this equation, $\phi_{i,k}$ is the kth component of ϕ_i, $r_k^{(n)}$ the kth component of $\mathbf{r}^{(n)}$, $S_{a,i}$ denotes the ith mean spectral pseudo-acceleration (i.e., the ordinate of the 5% damped mean pseudo-acceleration spectrum at the ith period $2\pi/\omega_i$), and m_{PGA} represents the mean peak ground acceleration. Note that in a planar frame structure with lumped masses the kth degree of freedom corresponds to the kth floor. This CQC rule is based on the assumptions of the normal stationary random vibration theory. For details we refer to [7,13].

The computation of the correlation coefficient between the ith and the jth modal total acceleration, $\rho_{i,j}$, the correlation coefficient between the ith modal and the ground acceleration, $\rho_{i,g}$, the peak factor of the ith modal total acceleration, p_i, the peak factor of the ground acceleration, p_{g}, and the peak factor of the response acceleration in the kth degree of freedom, p_k, is summarized in Appendix 1. As outlined in this Appendix, these quantities are expressed in terms of spectral and cross-spectral moments of the involved random variables [5]. The cross-spectral moment of order l between the ith and jth modal total accelerations is defined as [5]

$$\lambda_{l,ij} = \int_0^\infty \nu^l G_{\mathrm{g}}(\nu) H_i(\nu) H_j^*(\nu) \mathrm{d}\nu \qquad \text{for} \quad l = 0, 1, 2, \ldots, \tag{4}$$

where $H_i(\nu)$ is the transfer function (often referred to as frequency response function (FRF)) of the ith modal total acceleration $\ddot{d}_i(t)$,

$$H_i(\nu) = \frac{\omega_i^2 + 2\mathrm{i}\zeta_i \omega_i \nu}{\omega_i^2 - \nu^2 + 2\mathrm{i}\zeta_i \omega_i \nu}, \tag{5}$$

and the asterisk denotes the complex conjugate. $G_{\mathrm{g}}(\nu)$ represents the power spectral density (PSD) that characterizes the seismic hazard, $\ddot{u}_{\mathrm{g}}(t)$, in the frequency domain. In the present study the Kanai–Tajimi PSD, defined as [11,26]

$$G_{\mathrm{g}}^{(\mathrm{KT})}(\nu) = G_0 \frac{1 + 4\zeta_{\mathrm{g}}^2 \left(\nu/\nu_{\mathrm{g}}\right)^2}{\left(1 - \left(\nu/\nu_{\mathrm{g}}\right)^2\right)^2 + 4\zeta_{\mathrm{g}}^2 \left(\nu/\nu_{\mathrm{g}}\right)^2}, \tag{6}$$

is utilized as analytical mean PSD model of the base excitation. Therein, the normalized PSD of the underlying white noise process, G_0, the characteristic frequency of the ground motion, ν_{g}, and damping ratio of the ground, ζ_{g}, are calibrated to fit the seismic hazard of the considered site.

When evaluating the cross-spectral moment between the ith total modal acceleration and the ground acceleration, $\lambda_{l,ig}$ (i.e., $j \to g$), and the spectral moment $\lambda_{l,gg}$ (i.e., $i \to g$, $j \to g$), the FRF of the ground, $H_\mathrm{g} = 1$ (since $\lim_{\omega_i \to \infty} H_i(\nu) = H_\mathrm{g} = 1$), is substituted.

In contrast to the contribution of Pozzi and Der Kiureghian [17], where the cross-spectral moments have been evaluated numerically, in [12,13] analytical expressions for the required cross-spectral moments between modal total accelerations have been derived. These expressions are listed in Appendix 2.

3 Approximations of the response spectrum method

Response quantities due to earthquake excitation are assumed to be lognormally distributed [20,21]. This assumption holds true for spectral pseudo-accelerations as well. Hence, it is reasonable to use a median pseudo-acceleration response spectrum for modal combination instead of a mean response spectrum. As a consequence, in Eq. (3) the mean PFA, m_{PFA_k}, must be substituted by the median PFA denoted as $\breve{m}_{\mathrm{PFA}_k}$. This also implies that subsequently instead of mean peak factors and spectral mean pseudo-accelerations the corresponding median values are used, however, without changing the designation of the variables.

In this section, several approximations of the CQC modal combination rule for predicting median PFA demands according to (3) are proposed. The aim is to reduce the effort of analysis without significantly decreasing the accuracy of the response prediction.

The assumption that the ratios of the peak factors are unity,

$$\frac{p_k}{p_i} = \frac{p_k}{p_j} = \frac{p_k}{p_\mathrm{g}} = 1, \tag{7}$$

yields the approximated CQC rule with unit peak factor ratios (CQC-nopf) [17],

$$\breve{m}_{\mathrm{PFA}_k} \approx \left[\sum_{i=1}^{n} \sum_{j=1}^{n} \phi_{i,k} \Gamma_i S_{a,i} \phi_{j,k} \Gamma_j S_{a,j} \rho_{i,j} + \left(\breve{m}_{\mathrm{PGA}} r_k^{(n)} \right)^2 + 2 \breve{m}_{\mathrm{PGA}} r_k^{(n)} \sum_{i=1}^{n} \phi_{i,k} \Gamma_i S_{a,i} \rho_{i,\mathrm{g}} \right]^{\frac{1}{2}}. \tag{8}$$

Evaluation of the peak factors involves the computation of the first and the second cross-spectral moments in order to evaluate the first-passage probability (compare with Appendix 1), an effort which is not necessary when employing the CQC-nopf rule. Thus, application of this rule simplifies the prediction of the median PFA demand.

In a further simplification, the modal responses are assumed to be stochastically independent, yielding an extended SRSS rule with consideration of truncated modes,

$$\breve{m}_{\mathrm{PFA}_k} \approx \left[\sum_{i=1}^{n} \left(\frac{p_k}{p_i} \phi_{i,k} \Gamma_i S_{a,i} \right)^2 + \left(\frac{p_k}{p_\mathrm{g}} \breve{m}_{\mathrm{PGA}} r_k^{(n)} \right)^2 \right]^{\frac{1}{2}}, \tag{9}$$

$$\breve{m}_{\mathrm{PFA}_k} \approx \left[\sum_{i=1}^{n} \left(\phi_{i,k} \Gamma_i S_{a,i} \right)^2 + \left(\breve{m}_{\mathrm{PGA}} r_k^{(n)} \right)^2 \right]^{\frac{1}{2}}. \tag{10}$$

Modal combination according to Eq. (9) is referred to as SRSS rule with truncated modes and peak factors (t-SRSS-pf), and Eq. (10) as SRSS rule with truncated modes and unit peak factor ratios (t-SRSS-nopf).

When additionally the contribution of truncated modes is omitted, the above equations degenerate to

$$\breve{m}_{\mathrm{PFA}_k} \approx \left[\sum_{i=1}^{n} \left(\frac{p_k}{p_i} \phi_{i,k} \Gamma_i S_{a,i} \right)^2 \right]^{\frac{1}{2}}, \tag{11}$$

$$\breve{m}_{\mathrm{PFA}_k} \approx \left[\sum_{i=1}^{n} \left(\phi_{i,k} \Gamma_i S_{a,i} \right)^2 \right]^{\frac{1}{2}}. \tag{12}$$

Equation (12) is identical with the common SRSS rule [19], in this paper referred to as SRSS-nopf. Including the peak factors, Eq. (11), yields the modal combination SRSS rule with peak factors (SRSS-pf).

4 Approximations of the underlying cross-spectral moments

In Appendix 2, the analytical expressions of the underlying cross-spectral moments derived in [12,13] are listed. Approximation of the cross-sectional moments with respect to the exponent of the damping ratios makes also the evaluation of the median PFA demands less expensive.

4.1 First-order approximation of cross-spectral moments

Expansion of the sums in Eq. (36) to the first degree of the exponent of the damping ratios yields for the zeroth cross-spectral moment

$$\lambda_{0,ij}^{(1)} = G_0 \pi \omega_i \omega_j \nu_g \left[\frac{\sum_{m=0}^{1} \sum_{n=0}^{1} \zeta_i^m \zeta_j^n \xi_{0,mn}(\omega_i, \omega_j)}{4\zeta_g D_4} + \frac{2\nu_g \sum_{m=0}^{1} \sum_{n=0}^{1} \zeta_i^m \zeta_j^n \psi_{0,mn}(\omega_i, \omega_j)}{D_1} \right]. \quad (13)$$

This expression is equivalent to a successively first-order Taylor series expansion of the numerator of $\lambda_{0,ij}$, Eq. (36), at $\zeta_i = 0$ and $\zeta_j = 0$ with the benefit of explicitly using the readily developed functionals $\xi_{0,mn}(\omega_i, \omega_j)$, $\psi_{0,mn}(\omega_i, \omega_j)$, D_1, and D_4 presented in [12,13].

Analogously, the first and the second cross-spectral moments, Eqs. (38) and (37), respectively, are subjected to a first-order expansion with the result

$$\begin{aligned} \lambda_{1,ij}^{(1)} = G_0 \omega_i \omega_j \nu_g^2 \Bigg[& \omega_i \left(\frac{\pi}{2} - \zeta_i \right) \left(\frac{\sum_{m=0}^{1} \sum_{n=0}^{1} \zeta_i^m \zeta_j^n \psi_{1,mn}(\omega_i, \omega_j)}{D_1} \right) \\ & + \omega_j \left(\frac{\pi}{2} - \zeta_j \right) \left(\frac{\sum_{m=0}^{1} \sum_{n=0}^{1} \zeta_i^n \zeta_j^m \psi_{1,mn}(\omega_j, \omega_i)}{D_2} \right) \\ & + \ln(\omega_i)\, \omega_i \left(\frac{\sum_{m=0}^{1} \sum_{n=0}^{1} \zeta_i^m \zeta_j^n \hat{\psi}_{1,mn}(\omega_i, \omega_j)}{D_1} \right) \\ & + \ln(\omega_j)\, \omega_j \left(\frac{\sum_{m=0}^{1} \sum_{n=0}^{1} \zeta_i^n \zeta_j^m \hat{\psi}_{1,mn}(\omega_j, \omega_i)}{D_2} \right) \Bigg], \end{aligned} \quad (14)$$

$$\lambda_{2,ij}^{(1)} = G_0 \pi \omega_i \omega_j \nu_g^2 \left[\frac{\nu_g \sum_{m=0}^{1} \sum_{n=0}^{1} \zeta_i^m \zeta_j^n \xi_{2,mn}(\omega_i, \omega_j)}{4\zeta_g D_4} + \frac{2\omega_i^2 \sum_{m=0}^{1} \sum_{n=0}^{1} \zeta_i^m \zeta_j^n \psi_{2,mn}(\omega_i, \omega_j)}{D_1} \right], \quad (15)$$

in which the approximations $\sqrt{1-\zeta_i^2} \approx 1$ and $\arctan(\zeta_i) \approx \zeta_i$ are appropriate for small damping ratios. Since the third and the sixth terms of Eq. (37) do not significantly contribute to the first cross-spectral moment, these terms are not considered in $\lambda_{1,ij}^{(1)}$. The functionals $\psi_{1,mn}$, $\hat{\psi}_{1,mn}$ and D_2 are listed in [12,13].

The first-order expansion of polynomials in the numerator of $\lambda_{0,ig}$ results in

$$\lambda_{0,ig}^{(1)} = \frac{G_0 \pi \omega_i \nu_g}{4\zeta_g} \frac{\omega_i^3 - \omega_i \nu_g^2 + 4\omega_i^3 \zeta_g^2 + \zeta_i \left(4\omega_i^2 \nu_g \zeta_g + 4\nu_g^3 \zeta_g + 16\omega_i^2 \nu_g \zeta_g^3 \right)}{K(\nu_g, \zeta_g, -\omega_i, \zeta_i)}. \quad (16)$$

The functionals K can be found in [12,13].

The correlation coefficients and peak factors based on these first-order approximations of the cross-spectral moments are referred to as $\rho_{i,j}^{(1)}$, $\rho_{i,g}^{(1)}$, $p_k^{(1)}$ and $p_i^{(1)}$. Substituting the latter quantities into Eq. (3) instead of the exact analytical counterparts leads to the first-order approximation CQC rule (foa-CQC-pf).

The first-order approximation CQC rule with unit peak factor ratios (foa-CQC-nopf) denotes response spectrum analysis with unity peak factors according to Eq. (8) based on first-order approximations $\rho_{i,j}^{(1)}$ and $\rho_{i,g}^{(1)}$.

4.2 Hybrid approximation of cross-spectral moments

A preliminary study has shown that even a zeroth-order expansion of the first term in the brackets of Eq. (36) can be used to estimate the correlation coefficients. Accordingly, $\lambda_{0,ij}$, respectively, $\lambda_{0,ij}^{(1)}$ degenerates to

$$\lambda_{0,ij}^{(1')} = G_0 \pi \omega_i \omega_j \nu_g \left[\frac{\xi_0(\omega_i, \omega_j)}{4\zeta_g D_4} + \frac{2\nu_g \left(\zeta_i \psi_{0,10}(\omega_i, \omega_j) + \zeta_j \psi_{0,01}(\omega_i, \omega_j) \right)}{D_1} \right]. \tag{17}$$

$\lambda_{0,ij}^{(1')}$ is a hybrid type (or a blend) of a first-order and a zeroth-order approximation of $\lambda_{0,ij}$. The functionals $\xi_0(\omega_i, \omega_j) \equiv \xi_{0,00}(\omega_i, \omega_j)$, $\psi_{0,10}(\omega_i, \omega_j)$ and $\psi_{0,01}(\omega_i, \omega_j)$ present in this relation read

$$\xi_0 \left(\omega_i, \omega_j \right) = \omega_i \omega_j \left(\omega_i^2 \left(\omega_j^2 \left(4\zeta_g^2 + 1 \right) - \nu_g^2 \right) - \omega_j^2 \nu_g^2 + \nu_g^4 \left(1 - 8\zeta_g^2 \right) \right), \tag{18}$$

$$\psi_{0,10} \left(\omega_i, \omega_j \right) = \omega_j \left(2\omega_i^6 \nu_g^2 + \omega_j^2 \nu_g^6 + 4\omega_i^8 \zeta_g^2 + 8\omega_i^2 \omega_j^2 \nu_g^4 \zeta_g^2 - \omega_i^4 \nu_g^2 \left(2\nu_g^2 + \omega_j^2 \left(1 + 8\zeta_g^2 - 16\zeta_g^4 \right) \right) \right), \tag{19}$$

$$\psi_{0,01} \left(\omega_i, \omega_j \right) = \omega_i^3 \nu_g^6 + 4\omega_i^9 \zeta_g^2 + \omega_i^7 \nu_g^2 \left(1 - 4\zeta_g^2 \right)^2 + 2\omega_i^5 \nu_g^4 \left(-1 + 4\zeta_g^2 \right). \tag{20}$$

In the same manner, the first term in the brackets of Eq. (38) is subject of a zeroth-order expansion yielding the following hybrid first-order and zeroth-order approximation of $\lambda_{2,ij}$,

$$\lambda_{2,ij}^{(1')} = G_0 \pi \omega_i \omega_j \nu_g^2 \left[\frac{\nu_g \xi_2(\omega_i, \omega_j)}{4\zeta_g D_4} + \frac{2\omega_i^2 \left(\zeta_i \psi_{2,10}(\omega_i, \omega_j) + \zeta_j \psi_{2,01}(\omega_i, \omega_j) \right)}{D_1} \right] \tag{21}$$

with the functionals

$$\xi_2 \left(\omega_i, \omega_j \right) = \omega_i \omega_j \left(\nu_g^2 \left(\nu_g^2 - \omega_j^2 \left(1 + 4\zeta_g^2 \right) \right) + \omega_i^2 \left(-\nu_g^2 \left(1 + 4\zeta_g^2 \right) + \omega_j^2 \left(1 + 4\zeta_g^2 - 16\zeta_g^4 \right) \right) \right), \tag{22}$$

$$\psi_{2,10}(\omega_i, \omega_j) = \psi_{1,10}(\omega_i, \omega_j) - \psi_{0,10}(\omega_i, \omega_j) \quad \psi_{2,01}(\omega_i, \omega_j) = \psi_{1,01}(\omega_i, \omega_j) - \psi_{0,01}(\omega_i, \omega_j). \tag{23}$$

Correspondingly, the zeroth-order approximation of $\lambda_{0,ig}$ read

$$\lambda_{0,ig}^{(1')} = \frac{G_0 \pi \omega_i \nu_g}{4\zeta_g} \frac{\omega_i^3 - \omega_i \nu_g^2 + 4\omega_i^3 \zeta_g^2}{K(\nu_g, \zeta_g, -\omega_i, \zeta_i)}. \tag{24}$$

These hybrid approximations of the cross-spectral moments are used to derive estimates of the correlation coefficients and peak factors. For the so-called hybrid approximation CQC rule (ha-CQC-pf) these quantities (i.e., $\rho_{i,j}^{(1')}$, $\rho_{i,g}^{(1')}$, $p_k^{(1')}$, $p_i^{(1')}$) are utilized when evaluating Eq. (3). The hybrid approximation CQC rule with unit peak factor ratios (ha-CQC-nopf) is based on Eq. (8) using $\rho_{i,j}^{(1')}$ and $\rho_{i,g}^{(1')}$.

5 Application and assessment

5.1 Characterization of the seismic excitation

In various example problems, the accuracy of the various approximate modal combination rules is validated. As "exact" reference solutions serve the outcomes of a computationally more demanding response history analysis (RHA), where the coupled set of equations of motion, Eq. (1), is directly solved. RHA requires a set of ground motion records adjusted to the site-specific seismic hazard, which is usually defined in terms of the 5% damped pseudo-acceleration design response spectrum, S_{ad} [2].

In the present study, as an example the seismic hazard representative for Century City (Los Angeles, CA; 34.05366°N, 118.41339°W) is considered. In Fig. 1 the corresponding design response spectrum, S_{ad}, is shown by the bold solid line. The spectrum is linearly scaled to the design earthquake spectral response acceleration parameter at short periods (i.e., in the plateau domain of the response spectrum) $S_{\mathrm{DS}} = 2.00$ g. From the PEER NGA database [15], 92 site-compatible ground motion records have been selected providing that median and

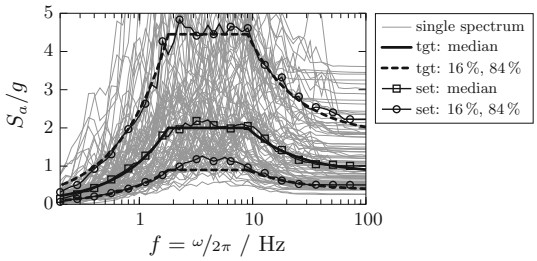

Fig. 1 Target response spectra (*bold black lines*), response spectra of individual records (*gray lines*) and statistical quantities (*lines with markers*) for a normal target dispersion $\sigma_t = 0.80$ [12]

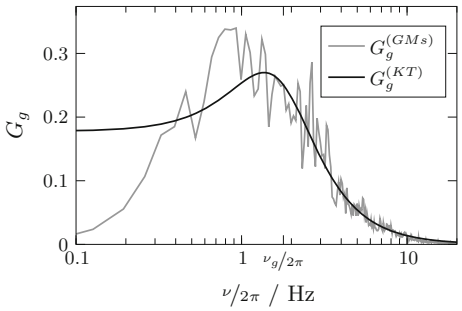

Fig. 2 Modeling the ground motion in the frequency domain. Kanai–Tajimi power spectral density (KT-PSD) (*black line*) fitted to the normalized median PSD of the ground motions (*gray line*) [12]

dispersion of the record set match this design response spectrum and a target dispersion of $\sigma_t = 0.80$ in the frequency range of $0.33\,\text{Hz} \leq \omega/2\pi \leq 20\,\text{Hz}$ (i.e., the period range of $0.05\,\text{s} \leq T \leq 3.00\,\text{s}$). The underlying evolutionary record selection algorithm is described in [14]. Additionally, Fig. 1 shows the target median ± one logarithmic standard deviation spectra (bold dashed lines), individual response spectra of the selected records (solid thin lines in gray) and the actual median, 16 and 84% quantile spectra (lines with markers).

The thin solid line in Fig. 2 corresponds to the normalized median of the individual PSDs of the selected ground motion records, $G_{\text{g}}^{(\text{GMs})}$, leaving the integral in the frequency range of $0.01\,\text{Hz} \leq \nu/2\pi \leq 20\,\text{Hz}$ to unity,

$$2\pi \int_{0.01}^{20} G_{\text{g}}^{(\text{GMs})} \text{d}\nu = \frac{2\pi}{SF} \int_{0.01}^{20} \overline{G}_{\text{g}}^{(\text{GMs})} \text{d}\nu = 1, \tag{25}$$

in which $\overline{G}_{\text{g}}^{(\text{GMs})}$ denotes the unscaled median of the individual PSDs of the selected ground motion records. In the present case the scale factor, SF, is 1.45. Calibration of the characteristic parameters in the KT-PSD model, Eq. (6), to the normalized median PSD of the records yields $G_0 = 0.18$, $\nu_{\text{g}}/2\pi = 1.79\,\text{Hz}$, and $\zeta_{\text{g}} = 0.78$.

5.2 Assessment of the approximations of the cross-spectral moments

Subsequently, the accuracy of the first-order and the hybrid approximations of the cross-spectral moments is assessed through comparison of the correlation coefficients, which are composed of the cross-spectral moments. This intuitive approach is consistent with [5]. Thus, in analogy to the physically meaningful zeroth correlation coefficients ($l = 0$), generic correlation coefficients composed of the first ($l = 1$) and the second ($l = 2$) cross-spectral moments are defined [5], compared with Eq. (29),

$$\rho_{l,i,j} = \frac{\lambda_{l,ij}}{\sqrt{\lambda_{l,ii}\lambda_{l,jj}}} \qquad \rho_{l,i,\text{g}} = \frac{\lambda_{l,i\text{g}}}{\sqrt{\lambda_{l,ii}\lambda_{l,\text{gg}}}} \qquad \text{for} \quad l = 0, 1, 2 \tag{26}$$

For $l = 1$ there is no meaningful physical interpretation of Eq. (26), but it is related to the envelope of the random process [6,27] in order to define the shape factor, q_{e} (Eq. (33)), to evaluate the first-passage probability (Eq. (32)). The second cross-spectral moment represents the mean square derivative of the random process

[6,27]. That is, the second cross-spectral moment can be geometrically interpreted as the slope of the random process.

It should be noted that for reasons discussed in [12] the first and the second correlation coefficient between the ith modal total acceleration and the ground acceleration is indefinite, compared with Eq. (40).

In the subsequent assessment, the correlation coefficients according to Eq. (26) are evaluated substituting the rigorous cross-spectral moments specified in Appendix 2 as well the their approximations derived in Sect. 4.

5.2.1 Correlation coefficients based on the zeroth spectral moments

Figure 3a, b provides graphical representations of the correlation coefficients $\rho_{i,j} \equiv \rho_{0,i,j}$ and their approximations, $\rho_{i,j}^{(1)} \equiv \rho_{0,i,j}^{(1)}$ and $\rho_{i,j}^{(1')} \equiv \rho_{0,i,j}^{(1')}$, to the filtered white noise input according to the KT-PSD model. The thick solid line represents the closed-form solution, and the approximations are indicated by dashed (first-order approximation) and dotted (hybrid-type approximation) lines. The abscissa shows angular frequency ω_i normalized by means of angular frequency ω_j in the range of the first lower and higher octave. For $w_j/2\pi = 4.0\,\text{Hz}$ (left column) and $w_j/2\pi = 8.0\,\text{Hz}$ (right column), respectively, the differences between the closed-form solution and various approximations of the correlation coefficients are relatively large and, therefore, appropriate for graphical visualization. It is of relevance to note that the approximated correlation coefficients for $4.0\,\text{Hz} \geq \omega_j \geq 8.0\,\text{Hz}$ literally match the closed-form solution [12]. However, sharp spikes are a result of a very small damping ratio of 0.01, regardless of angular frequency ω_j and the degree of simplification, as shown by the lines with circular markers. If the damping ratio was zero, the bell shape would degenerate to the normalized Dirac delta function. This can be explained by the fact that modal response quantities represent orthogonal signals. Increasing the damping ratio smoothens the bell shape, indicating that modal accelerations are highly correlated regardless of angular frequency ω_j, see for example in Fig. 3b the solid black line with diamond markers representing the correlation coefficient for $\zeta_i = \zeta_j = 0.20$.

The results show that all approximations of the correlation coefficients are in excellent agreement with the exact solution, however derived with less computational effort. For small damping ratios ($\zeta \leq 0.05$), the approximations literally match the closed-form solution (compare lines with circular and triangular markers). Even for large damping ratios up to $\zeta = 0.20$ the approximations are reasonably accurate (compare lines with square and diamond markers).

In Fig. 4 the correlation coefficients between modal total acceleration and ground acceleration, $\rho_{0,i,g}$, the corresponding first-order approximation, $\rho_{0,i,g}^{(1)}$, and the hybrid approximation $\rho_{0,i,g}^{(1')}$ are shown. This comparison reveals that both approximations are accurate for damping ratios up to $\zeta \leq 0.05$, as it is the case in standard civil engineering structures.

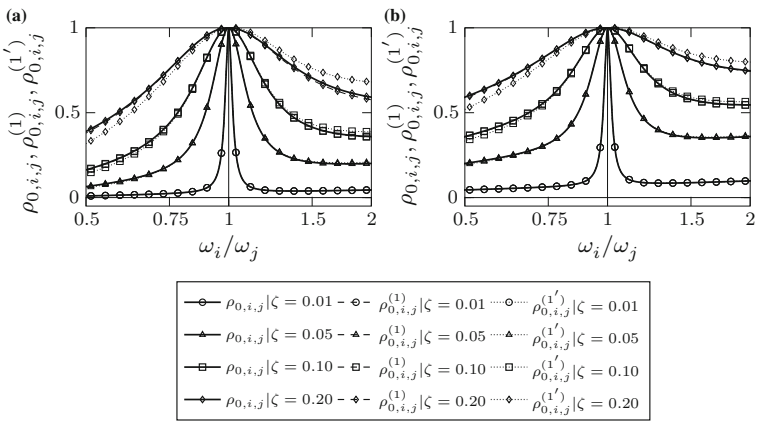

Fig. 3 Correlation coefficients $\rho_{0,i,j}$ and their approximations $\rho_{0,i,j}^{(1)}$ and $\rho_{0,i,j}^{(1')}$ for different damping ratios $\zeta = \zeta_i = \zeta_j$, evaluated for frequencies **a** $\omega_j/2\pi = 4.0\,\text{Hz}$ and **b** $\omega_j/2\pi = 8.0\,\text{Hz}$

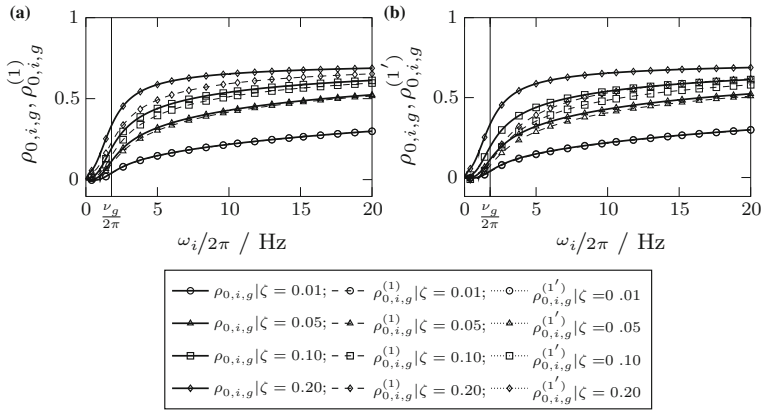

Fig. 4 Correlation coefficients $\rho_{0,i,g}$ and their approximations $\rho^{(1)}_{0,i,g}$ and $\rho^{(1')}_{0,i,g}$ for different damping ratios ζ_i

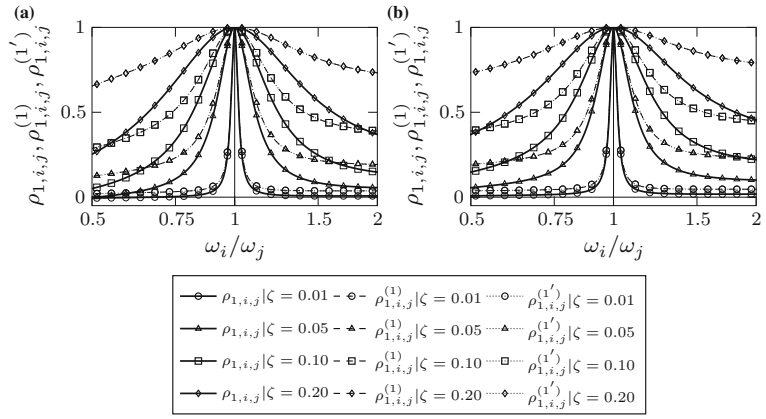

Fig. 5 Correlation coefficients $\rho_{1,i,j}$ and their approximations $\rho^{(1)}_{1,i,j}$ and $\rho^{(1')}_{1,i,j}$ for different damping ratios $\zeta = \zeta_i = \zeta_j$, evaluated for frequencies **a** $\omega_j/2\pi = 4.0\,\text{Hz}$ and **b** $\omega_j/2\pi = 8.0\,\text{Hz}$

5.2.2 Correlation coefficients based on the first and second spectral moments

The correlation coefficients based on the first and second spectral moments, $\rho_{1,i,j}$ and $\rho_{2,i,j}$, respectively, and their corresponding approximations, $\rho^{(1)}_{1,i,j}$ and $\rho^{(1')}_{1,i,j}$, and $\rho^{(1)}_{2,i,j}$ and $\rho^{(1')}_{2,i,j}$, respectively, are depicted in Figs. 5a, b and 6a, b as function of frequency ratio ω_i/ω_j. Solid lines correspond to the evaluations of the exact expression of the correlation coefficients, dashed lines to the first-order approximations and the dotted lines to the hybrid approximations.

It is observed that the difference between $\rho_{1,i,j}$ and its approximations $\rho^{(1)}_{1,i,j}$ and $\rho^{(1')}_{1,i,j}$ becomes larger as ω_i increases. However, in the resonance domain ($\omega_i \approx \omega_j$) the approximations are very close to the exact counterpart. Since the underlying approximations of the first cross-spectral moments are identical, also $\rho^{(1)}_{1,i,j}$ and $\rho^{(1')}_{1,i,j}$ are identical.

Both the first-order and the hybrid approximations of the correlation coefficients based on the second spectral moments provide in the entire frequency range an excellent estimate for relatively small damping ratios up to $\zeta \leq 0.05$. In the frequency range $\omega_j/2\pi \geq 4.0\,\text{Hz}$ the approximations literally match the exact solution regardless of the damping coefficient.

The results discussed herein indicate that for damping ratios $\zeta \leq 0.05$ the correlation coefficients can be estimated sufficiently accurate utilizing the proposed approximations of first and second cross-spectral moments according to Eqs. (14) and (15), respectively, Eq. (21) with less computational effort.

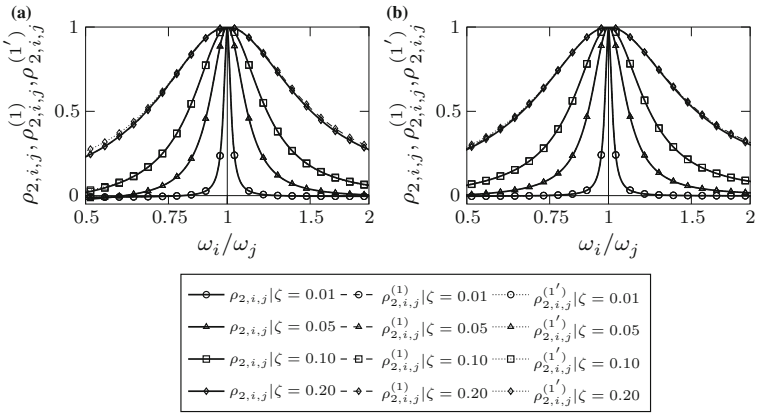

Fig. 6 Correlation coefficients $\rho_{2,i,j}$ and their approximations $\rho^{(1)}_{2,i,j}$ and $\rho^{(1')}_{2,i,j}$ for different damping ratios $\zeta = \zeta_i = \zeta_j$, evaluated for frequencies **a** $\omega_j/2\pi = 4.0\,\text{Hz}$ and **b** $\omega_j/2\pi = 8.0\,\text{Hz}$

5.3 Studied structural models

The proposed simplifications of the CQC rule for predicting the PFA demand are evaluated utilizing spatial 6-story, 12-story and 24-story generic structures. Each floor of these structural models is composed of four massless columns and a horizontal rigid diaphragm, to which an eccentric lumped mass is assigned. The lumped mass at the roof level is only half of the lumped mass at the story levels within the building. Two types of structures are considered: steel moment-resisting frame (referred to as SMRF) structures and structures composed of shear walls (referred to as WALL). Each column of an SMRF structure is modeled as a simple beam-column element with discrete elastic springs at both ends, representing the flexural stiffness of the story beams. The models of the WALL structures are composed of the same elements; however, they are stiffer in the lateral direction than SMRFs. Consequently, the modal properties of SMRF and WALL generic structures are also different: The fundamental mode shape of a symmetric SMRF structure (i.e., the lumped masses are centered) is assumed to be linear, while for a symmetric WALL structure a parabolic shape with respect to the height is assumed. In the considered generic spatial structures the center of mass of each rigid floor is eccentric with respect to the center of stiffness: $\mathbf{e}_M = [x = 0.30, y = 0.30\,\text{m}]^\intercal$ (schematically depicted in Fig. 7a). Thus, these structures exhibit closely spaced modes, which is desirable for evaluation of the proposed CQC modal combination rules. Figure 7b shows a sketch of the lower stories of these structures. The fundamental frequencies of the structures match the values specified in ASCE 7-10 [2]. The first three angular natural frequencies are: $\omega_1 = 7.20, \omega_2 = 7.33, \omega_3 = 7.96\,\text{rad}\,\text{s}^{-1}$ (6-story SMRF); $\omega_1 = 4.14, \omega_2 = 4.21, \omega_3 = 4.59\,\text{rad}\,\text{s}^{-1}$ (12-story SMRF); $\omega_1 = 2.38, \omega_2 = 2.42, \omega_3 = 2.64\,\text{rad}\,\text{s}^{-1}$ (24-story SMRF); $\omega_1 = 12.58, \omega_2 = 12.59, \omega_3 = 31.48\,\text{rad}\,\text{s}^{-1}$ (6-story WALL); $\omega_1 = 7.55, \omega_2 = 7.55, \omega_3 = 30.95\,\text{rad}\,\text{s}^{-1}$ (12-story WALL); $\omega_1 = 4.49, \omega_2 = 4.49, \omega_3 = 28.2\,\text{rad}\,\text{s}^{-1}$ (24-story WALL). Rayleigh-type damping is considered with a modal damping ratio of $\zeta = 0.05$ assigned to the fundamental mode and to the 95% cumulative mass participating mode. Further details to these structures are found in [12].

5.4 Results

The "exact" median PFA demands computed by RHA serve as benchmark solution, exposing the structures in x-direction to the 92 ground motions of the Century City record set. That is, each support is excited by the same ground acceleration series, which represents the second derivative of ground displacement u_{xg}. Exemplary, the PFA demand is shown for x-component of corner point A, see Fig. 7, and denoted as PFA_k in the kth floor level. To these PFA demands, the outcomes of the various modal combination rules are set in contrast and subsequently assessed.

Figures 8, 9, 10, 11 show the predicted median PFA demands in terms of profiles with respect to the normalized building height h_{rel}. The plots of the first row refer to the 6-story, of the second row to the 12-story and of the third row to the 24-story structures. In the plots of the left column results of the various CQC methods based on a single-mode approximation are shown, and the outcomes of the right column include all modes up to the 95% cumulative mass participating mode. Gray solid lines depict the median PFA demands obtained from RHA.

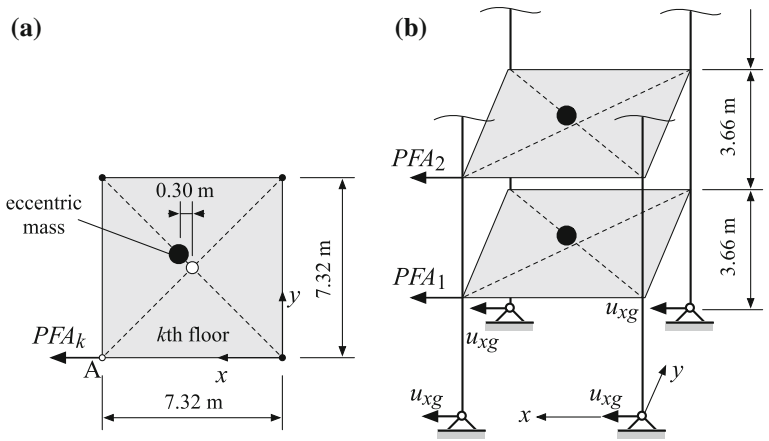

Fig. 7 **a** Plane view of the eccentric mass at the *k*th floor level and **b** isometric view of the first two stories of the spatial structure [13]

5.4.1 Median peak floor acceleration demand based on modal combination rules considering peak factors

Figures 8 and 9 show the outcomes of the CQC-pf modal combination rule and its simplified counterparts considering peak factors (i.e., foa-CQC-pf rule, ha-CQC-pf rule, t-SRSS-pf rule, SRSS-pf rule). These outcomes are set in contrast to the median PFA demands from RHA.

The most important result of this study is that for both WALL and SMRF structures the full CQC (CQC-pf) method predicts quite accurately the PFA demands when all modes up to the 95% mass participating mode are included, see subfigures (b), (d) and (f) of Figs. 8 and 9. Going into more detail, it is observed that for the considered SMRF structures and the 6-story WALL structure the CQC-pf method underestimates only slightly the RHA benchmark solution along the entire structural height. The median PFA demands of the 12-story and the 24-story WALL structure exhibit a distinct S-shape that is quite accurately approximated by the CQC-pf rule. However, in the 24-story structure modal combination according to this rule overestimates the amplitude of the PFA demand in the domain of this S-shape.

Another important observation is that the loss of accuracy is small when using the CQC rules in a multi-modal approach based on first-order (foa-CQC-pf rule) or hybrid approximations (ha-CQC-pf rule) of the cross-spectral moments, as shown in the right column of Figs. 8 and 9. Only for the SMRF structures these simplified rules lead to a minor apparent underestimation of the PFA profiles, see subfigures (a). It is of relevance to emphasize the simple application of the foa-CQC-pf and ha-CQC-pf rules, because in contrast the full CQC-pf rule evaluation of the functionals concerning the zeroth and first exponent of the damping ratio is required only. It can be, thus, concluded that for PFA assessment in civil engineering structures, where damping is relatively low (i.e., $\zeta \leq 5\%$), both the foa-CQC-pf and the ha-CQC-pf rule can be used instead of the full CQC-pf method, however, with less effort but without crucial loss of accuracy.

The SRSS method considering truncated modes and peak factors (t-SRSS-pf) and the common SRSS method with peak factors (SRSS-pf) are not capable of capturing the actual magnitude of the median PFA demand of the considered spatial structures, regardless of the type of lateral load-bearing system and the number of stories. The magnitude is in general underestimated by about 20–30%. These outcomes show the importance of the correlation coefficients between modal total accelerations, and it can be concluded that the correlation coefficients contribute significantly to the peak response if the modes are closely spaced.

The t-SRSS-pf rule provides only a sufficient accurate estimation of the *shape* of the PFA profiles when using all modes up to the 95% mass participating mode. It is also seen that considering truncated modes is important for PFA demand prediction in the lower story, compare the outcomes of the t-SRSS-pf and the SRSS-pf modal combination rules.

In contrast, for *planar* frame structures the t-SRSS-pf rule leads to satisfactory PFA predictions because the modes are well separated, as is comprehensively discussed in [12,13].

The single-mode approximations of all discussed modal combinations rules cannot capture the PFA demand of the considered spatial structures, as is seen from the outcomes shown in the left column of Figs. 8 and 9, even not for the mid-rise 6-story configurations. This demonstrates the importance of the contribution of higher modes on the PFA demand, in particular if modes are closely spaced as it is the case here. Except for the SRSS

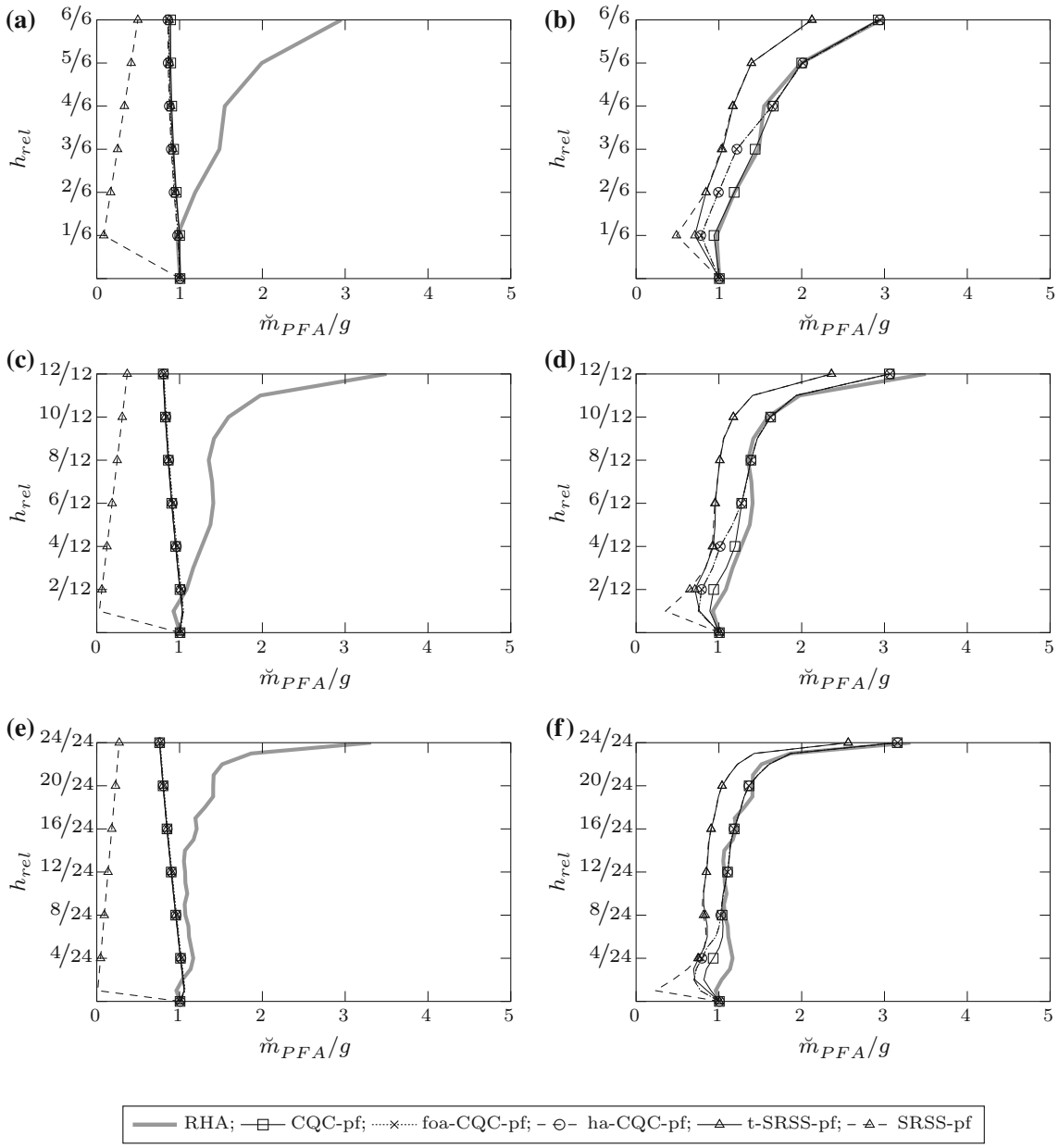

Fig. 8 Median PFA demand profiles for spatial SMRF structures with 6-stories (*first row*), 12-stories (*second row*) and 24-stories (*third row*). Benchmark solution based on RHA. Outcomes based on the full CQC rule considering peak factors (CQC-pf) and on various modal combination rules considering peak factors with first mode (*left column*) and 95% cumulative mass participating modes approximations (*right column*)

rule without truncated modes, all other methods based on the fundamental mode only yield the same perverted PFA demand prediction.

5.4.2 Median peak floor acceleration demand based on modal combination rules neglecting peak factors

Here, the proposed modal combination rules with unit peak factor ratios (i.e., CQC-nopf rule, foa-CQC-nopf rule, ha-CQC-nopf rule, t-SRSS-nopf rule, SRSS-nopf rule) are assessed. From Figs. 10 and 11 the following observations are made.

In a multi-modal approach up to the 95% mass participating mode the full CQC rule without peak factors (CQC-nopf rule) and its counterparts based on a first-order (foa-CQC-nopf rule) or a hybrid approximation

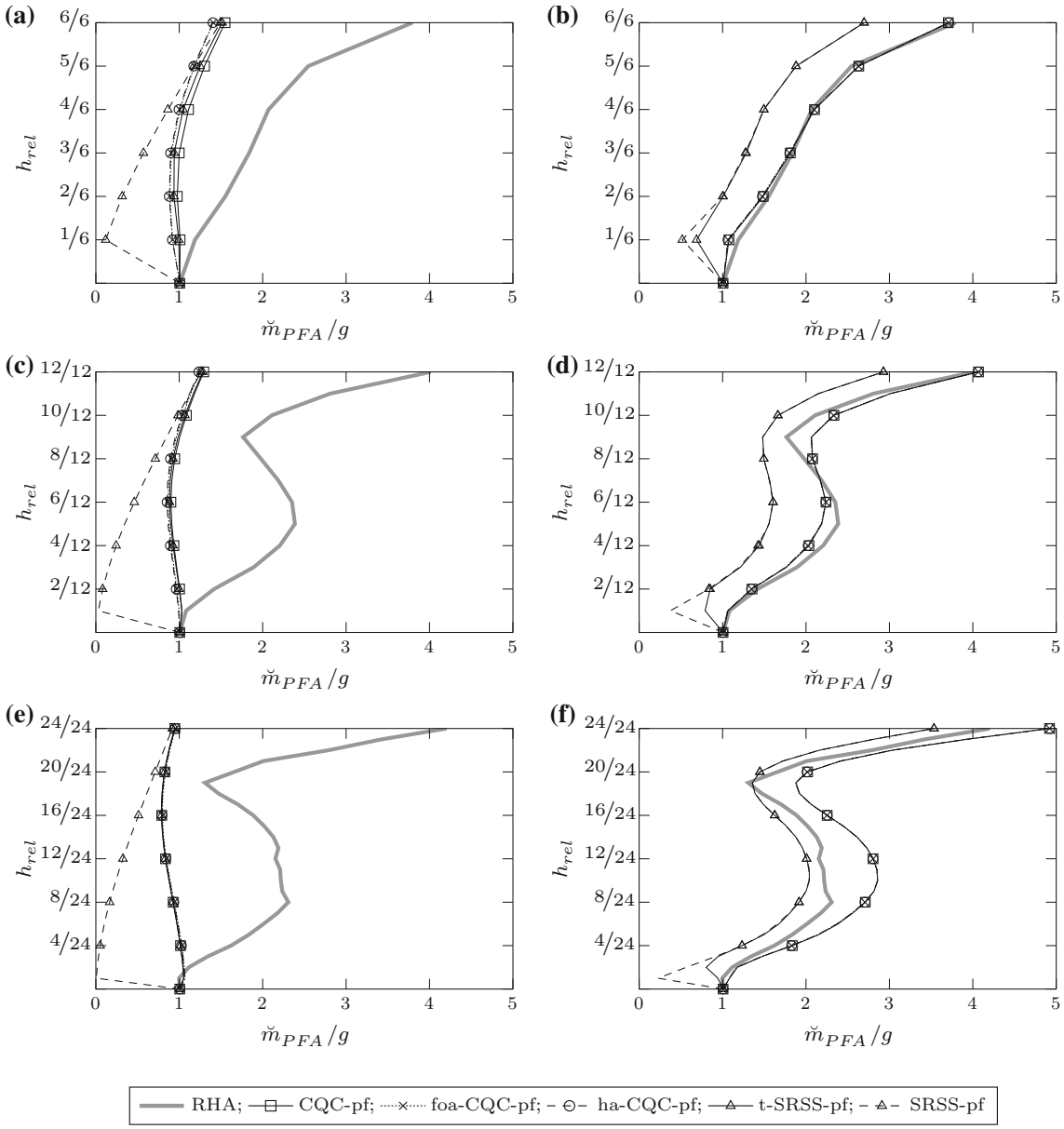

Fig. 9 Median PFA demand profiles for spatial WALL structures with 6-stories (*first row*), 12-stories (*second row*) and 24-stories (*third row*). Benchmark solution based on RHA. Outcomes based on the full CQC rule considering peak factors (CQC-pf) and on various modal combination rules considering peak factors with first mode (*left column*) and 95% cumulative mass participating modes approximations (*right column*)

(ha-CQC-nopf rule) of the underlying cross-spectral moments yield predictions of the median PFA demand that are in feasible agreement, see the plots of the right column of these figures. However, comparing these outcomes with the RHA benchmark solution shows that the PFA demand is significantly underestimated by these methods, revealing that for these structures the contribution of the peak factors should not be omitted. It is also observed that with increasing number of stories, consideration of the peak factors becomes more important for PFA demand assessment. This is an important observation for engineering practice because in general many structures respond in three dimensions although their seismic demand is predicted based on planar structural models.

The results in the left column of Figs. 10 and 11 also show that a first-mode approximation of the PFA demand underestimates the actual response significantly, regardless of the used modal combination rule and the considered structural configuration. The first-mode approximation of the common SRSS method (SRSS-nopf

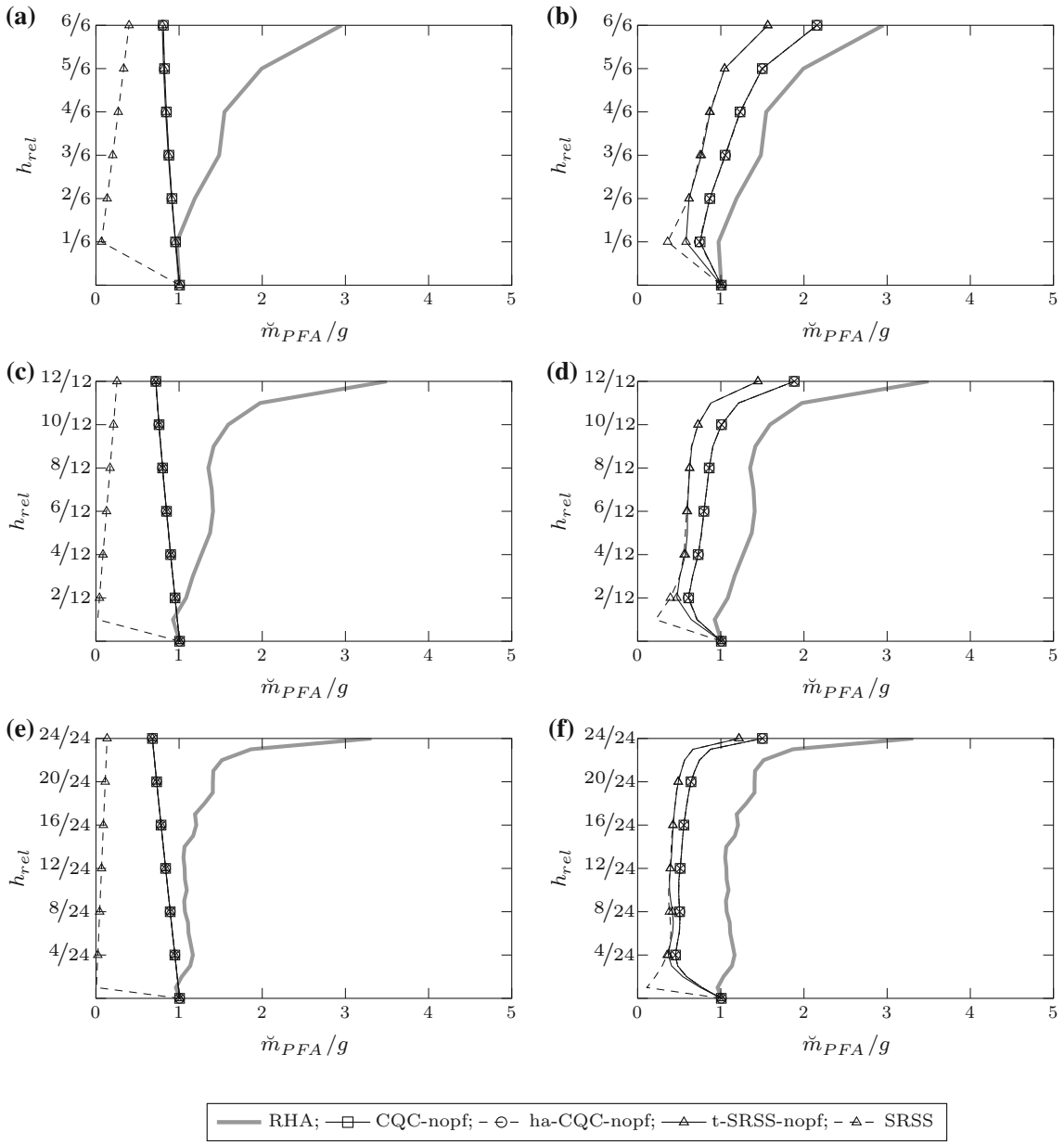

Fig. 10 Profiles of the median PFA demand for the spatial SMRF structures with 6-stories (*first row*), 12-stories (*second row*) and 24-stories (*third row*). Reference solution based on RHA, the full CQC rule neglecting peak factors (CQC-nopf) and various modal combination rules neglecting peak factors based on first mode (*left column*) and first to 95% cumulative mass participating mode approximation (*right column*)

rule) according to Eq. (12) follows the shape of the first mode, and thus, the corresponding PFA demands are furthest from the RHA benchmark solution. In a multi-mode approximation the results in the upper stories of the classical SRSS rule and the SRSS rule with truncated modes (t-SRSS-nopf) are almost identical. It is also observed that the impact of peak factors on the first-mode approximation is negligible for both the SMRF structures (compare Figs. 8a, c, e and 10a, c, e) and the WALL structures (compare Figs. 9a, c, e and 11a, c, e).

5.4.3 Error quantification

In Table 1 the error of the estimated median PFA demand of all considered modal combination rules with respect to the response history benchmark solution is quantified for each application example. The utilized

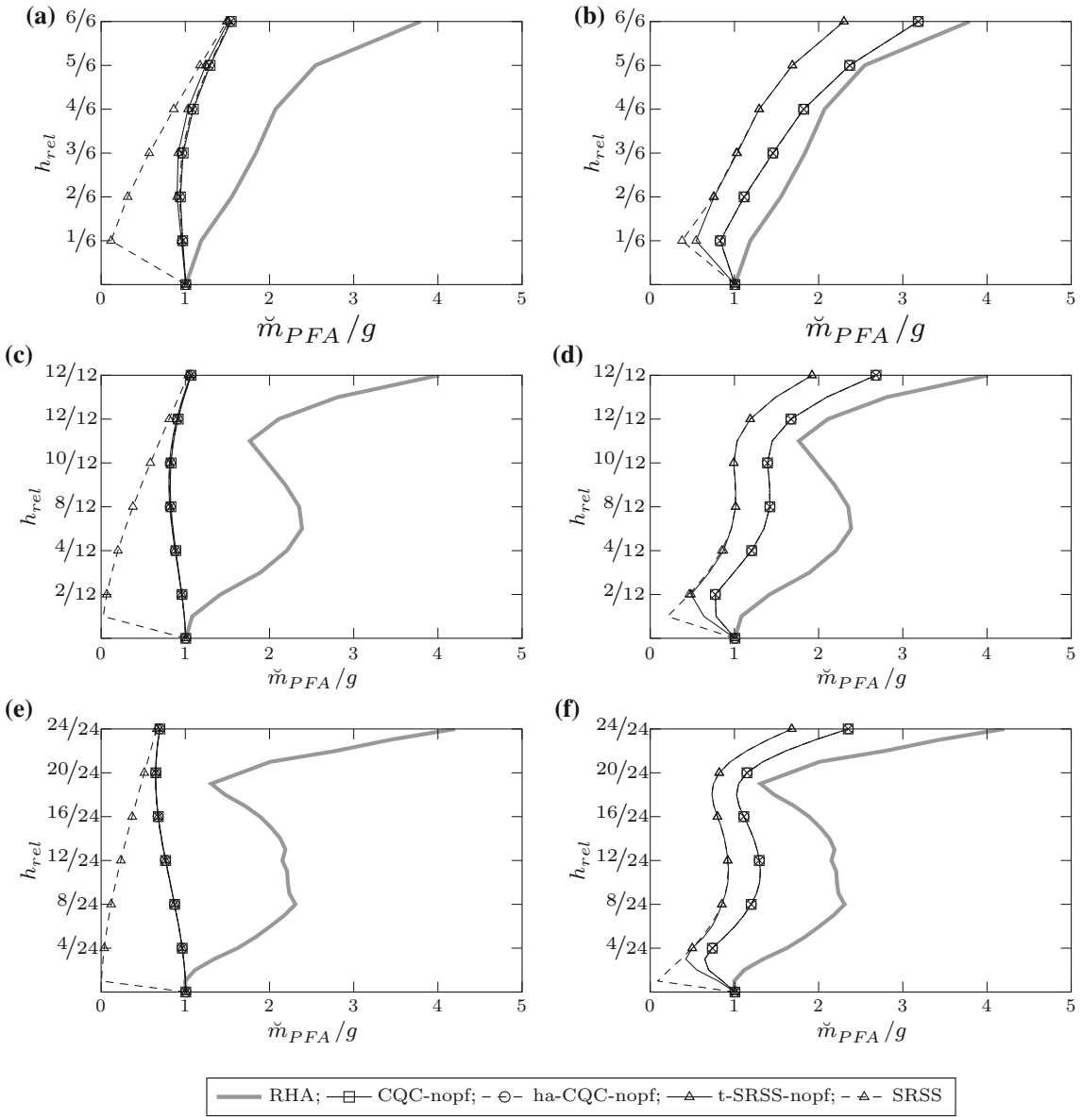

Fig. 11 Profiles of the median PFA demand for the spatial WALL structures with 6-stories (*first row*), 12-stories (*second row*) and 24-stories (*third row*). Reference solution based on RHA, the full CQC rule neglecting peak factors (CQC-nopf) and various modal combination rules neglecting peak factors based on first mode (*left column*) and first to 95% cumulative mass participating mode approximation (*right column*)

measure is the root-mean-square (RMS) error

$$m_\varepsilon = \sqrt{\frac{1}{N}\sum_{k=1}^{N}\varepsilon_k^2} \tag{27}$$

composed of the relative error of each floor acceleration component, defined as

$$\varepsilon_k = \frac{\breve{m}^{(\mathrm{mcr})}_{\mathrm{PFA}_k} - \breve{m}^{(\mathrm{RHA})}_{\mathrm{PFA}_k}}{\breve{m}^{(\mathrm{mcr})}_{\mathrm{PFA}_k}}, \tag{28}$$

Table 1 Root-mean-square error in %

Modal superposition rule	Considered modes	SMRF/stories			WALL/stories		
		6	12	24	6	12	24
CQC-pf	1	114	115	84	90	126	151
	2	45	79	87	32	84	112
	95%	3	8	11	5	7	17
foa-CQC-pf	1	119	113	83	108	135	149
	2	48	77	86	44	91	110
	95%	16	18	20	5	7	17
ha-CQC-pf	1	121	114	84	110	137	150
	2	49	78	87	45	93	112
	95%	16	18	20	5	7	17
t-SRSS-pf	1	117	116	85	97	129	152
	2	79	117	127	71	122	152
	95%	39	40	34	49	44	20
SRSS-pf	1	613	1159	2258	426	1227	3926
	2	183	417	882	276	845	2755
	95%	55	63	78	66	69	74
CQC-nopf	1	131	134	100	92	154	202
	2	73	136	212	34	107	155
	95%	34	68	115	28	60	76
ha-CQC-nopf	1	131	134	100	93	155	202
	2	73	136	212	34	108	155
	95%	34	68	115	28	60	76
t-SRSS-nopf	1	134	134	100	100	158	202
	2	114	188	281	73	152	204
	95%	85	122	171	83	125	146
SRSS	1	785	1720	4625	427	1509	5464
	2	249	639	1820	276	1043	3840
	95%	107	159	252	111	177	268

Reference solution from response history analysis (RHA)

where $\breve{m}^{(\mathrm{mcr})}_{\mathrm{PFA}_k}$ is the median PFA demand prediction of the kth floor from application of a modal combination rule, and $\breve{m}^{(\mathrm{RHA})}_{\mathrm{PFA}_k}$ is the corresponding outcome from response history analysis.

A major finding is that the error-based one, respectively, two-mode approximation is in all cases prohibitively large.

As already observed previously, the full CQC-pf rule including all modes up to the 95% mass participating mode yields for all structures the most accurate PFA demand prediction: For the 6-story SMRF structure, the RMS relative error is only 3%, for the 12-story structure, it is 8%, and for the 24-story structure, it increases to 11%. The error for the WALL structures is slightly larger, i.e., 5% for the 3-story and 17% for the 24-story structure.

Moreover, it is confirmed that the computationally relatively cheap first-order CQC (foa-CQC-pf) and hybrid CQC (ha-CQC-pf) methods considering peak factors yield feasible approximations of the PFA demand. While for the WALL structures the RMS error based on these approximations is of the same order as for CQC-pf rule, for the SMRF structures the error becomes, however, much larger, compare 11% for the 24-story SMRF based on the CQC-pf rule and 20% based on both the foa-CQC-pf and ha-CQC-pf rule.

The truncated SRSS rule considering peak factors with a maximum error of about 49% might be used in the pre-design phase of a structure for a quick estimate of the order of the PFA demands.

The remaining modal superposition methods are associated with large errors up to 268% (SRSS rule for the 24-story WALL structure). This clearly emphasizes the importance of considering correlation coefficients and peak factors when using modal combination rules for the simplified PFA demand prediction in spatial structures.

The RMS errors of the various discussed approximations modal superposition rules compared to the full CQC-pf rule listed in Table 2 underline these findings.

6 Summary and conclusions

The prediction of median peak floor (PFA) acceleration demands of spatial structures exposed to ground motions in one horizontal direction by means of various modal combination rules has been studied. The

Table 2 Root-mean-square error in %

Modal superposition rule	Considered modes (%)	SMRF/stories			WALL/stories		
		6	12	24	6	12	24
foa-CQC-pf	95	13	11	8	1	0	0
ha-CQC-pf	95	14	11	8	1	0	0
t-SRSS-pf	95	39	33	27	44	42	41
SRSS-pf	95	53	55	68	58	67	89
CQC-nopf	95	34	59	106	23	56	110
ha-CQC-nopf	95	34	59	106	23	56	110
t-SRSS-nopf	95	85	110	162	77	121	193
SRSS	95	106	146	231	101	172	313

Reference solution from CQC-pf rule

outcomes of response history analysis have been used as benchmark solutions to proof the accuracy of these response spectrum methods of various sophistication. The most accurate considered method is a comprehensive complete-quadratic-combination (CQC) rule with closed-form expressions for the involved correlation coefficients and peak factors. The proposed simplified versions of this rule represent either first-order or hybrid Taylor series expansions of the underlying cross-spectral moments, or peak factors, modal correlation and truncated modes are successively neglected, arriving finally at the classical and well-known square-root-of-sum-of-squares (SRSS) method.

The results presented in this contribution show that for the prediction of median PFA demands of tall *spatial* structures (here twelve and 24 stories) with closely spaced modes only modal combination rules considering correlation coefficients and peak factors yield reliable results. In the spatial structural systems with six stories, the contribution of the peak factors on the PFA demand is less pronounced. In contrast, previous studies have revealed that the PFA demands of *planar* structures can be predicted by modal combination rules without correlation coefficients. In the lower stories, truncated modes contribute significantly to the median PFA demand.

From the results, it can also be concluded that for PFA assessment in commonly damped civil engineering structures both the CQC methods based on first-order or hybrid Taylor series expansions of the underlying cross-spectral moments can be used instead of the full CQC method, however, with less computational effort.

Acknowledgements Open access funding provided by University of Innsbruck and Medical University of Innsbruck. L. Moschen conducted the research for this paper as student of the Doctoral School (FWF DK-PLUS) *Computational Interdisciplinary Modelling*, which is based at the University of Innsbruck, Austria, and substantially funded by the Austrian Science Fund (FWF). Additionally, this study was partially supported by the Austrian Ministry of Science BMWF as part of the *UniInfrastrukturprogramm* of the Focal Point Scientific Computing at the University of Innsbruck, Austria.

Appendix 1: Correlation coefficients and peak factors

This appendix provides a summary of evaluation of the required correlation coefficients and the peak factors required to determine the mean PFA demand according to the proposed CQC rules.

The correlation coefficients $\rho_{i,j}$ and $\rho_{i,\mathrm{g}}$ present in Eq. (3) can be expressed in terms of the corresponding zeroth spectral and cross-spectral moments [4],

$$\rho_{i,j} = \frac{\lambda_{0,ij}}{\sqrt{\lambda_{0,ii}\lambda_{0,jj}}}, \qquad \rho_{i,\mathrm{g}} = \frac{\lambda_{0,i\mathrm{g}}}{\sqrt{\lambda_{0,ii}\lambda_{0,\mathrm{gg}}}}. \tag{29}$$

The evaluation of the peak factors p_k, p_i and p_{g} is based on the common assumption of the first-passage probability for normal stationary random processes $X(t)$ with zero mean as proposed by Vanmarcke [28]. For details it is referred to [4,5,13,27,28].

The ith modal peak factor, p_i, and the peak factor of the ground acceleration p_g are determined according to [28]

$$p_i = \frac{S_\mathrm{a}(\omega_i)}{\lambda_{0,ii}}, \quad p_\mathrm{g} = \frac{S_\mathrm{a}(\omega_i \to \infty)}{\lambda_{0,\mathrm{gg}}} \tag{30}$$

with the readily available pseudo-acceleration response spectrum S_a and the spectral moments $\lambda_{0,ii}$ and $\lambda_{0,\mathrm{gg}}$.

The peak factor p_k is the outcome of the integral

$$p_k = E[R] = \int_0^\infty (1 - F_R(r))\,\mathrm{d}r, \tag{31}$$

where F_R is the first-passage probability [28],

$$F_R(r) = P[R \le r] = \left(1 - \exp\left(-\frac{r^2}{2}\right)\right) \exp\left(\frac{-2 f_a t \left(1 - \exp\left(-\sqrt{\frac{\pi}{2}} q_e r\right)\right)}{1 - \exp\left(-\frac{r^2}{2}\right)}\right). \tag{32}$$

In this equation, f_a denotes the mean rate of B-crossings [18], defined as crossings of the barrier level from below [28], and q_e is an empirical shape factor of the PSD of the response process [28],

$$f_a = \frac{1}{2\pi}\sqrt{\frac{\lambda_{2,k}}{\lambda_{0,k}}} \exp\left(\frac{-r^2}{2}\right), \quad q_\mathrm{e} = \left(1 - \frac{\lambda_{1,k}^2}{\lambda_{0,k}\lambda_{2,k}}\right)^{b/2}, \tag{33}$$

with $b = 1.20$. An appropriate approximation of the first-passage time, t, appearing in Eq. (32) is the average period of the response process, T_0, defined as [13]

$$T_0 = \frac{2\pi}{\sqrt{\frac{\lambda_{2,k}}{\lambda_{0,k}}}}. \tag{34}$$

Evaluation of Eqs. (33) and (34) requires the zeroth, first and second spectral moment of the corresponding random acceleration process based on the following first three multi-modal spectral moments [13]:

$$\lambda_{l,k} \approx \sum_{i=1}^{n}\sum_{j=1}^{n} \phi_{i,k}\Gamma_i\phi_{j,k}\Gamma_j\lambda_{l,ij}, \quad l = 0, 1, 2. \tag{35}$$

Appendix 2: Cross-spectral moments between modal total accelerations

The zeroth, first and second cross-spectral moment between modal total accelerations, $\lambda_{0,ij}$, $\lambda_{1,ij}$ and $\lambda_{2,ij}$, respectively, derived in [12,13] are recapitulated,

$$\lambda_{0,ij} = G_0\pi\omega_i\omega_j\nu_\mathrm{g}\left[\frac{\sum_{m=0}^{2}\sum_{n=0}^{2}\zeta_i^m\zeta_j^n\xi_{0,mn}(\omega_i,\omega_j)}{4\zeta_\mathrm{g}D_4} + \frac{2\nu_\mathrm{g}\sum_{m=0}^{4}\sum_{n=0}^{2}\zeta_i^m\zeta_j^n\psi_{0,mn}(\omega_i,\omega_j)}{D_1}\right], \tag{36}$$

$$\begin{aligned}
\lambda_{1,ij} = {} & G_0\omega_i\omega_j\nu_\mathrm{g}^2\left[\omega_i\left(\frac{\pi}{2} - \arctan\left(\frac{\zeta_i}{\sqrt{1-\zeta_i^2}}\right)\right)\left(\frac{\sum_{m=0}^{6}\sum_{n=0}^{2}\zeta_i^m\zeta_j^n\psi_{1,mn}(\omega_i,\omega_j)}{\sqrt{1-\zeta_i^2}D_1}\right)\right. \\
& + \omega_j\left(\frac{\pi}{2} - \arctan\left(\frac{\zeta_j}{\sqrt{1-\zeta_j^2}}\right)\right)\left(\frac{\sum_{m=0}^{6}\sum_{n=0}^{2}\zeta_i^n\zeta_j^m\psi_{1,mn}(\omega_j,\omega_i)}{\sqrt{1-\zeta_j^2}D_2}\right) \\
& + \left(\arctan\left(\frac{\zeta_\mathrm{g}}{\sqrt{1-\zeta_\mathrm{g}^2}}\right) - \frac{\pi}{2}\right)\left(\frac{\sum_{m=0}^{2}\sum_{n=0}^{2}D_4\zeta_i^m\zeta_j^n\xi_{1,mn}(\omega_i,\omega_j) + D_3\zeta_i^n\zeta_j^m\xi_{1,mn}(\omega_j,\omega_i)}{4\zeta_\mathrm{g}\sqrt{1-\zeta_\mathrm{g}^2}D_3D_4}\right) \\
& \left. + \omega_i\ln(\omega_i)\left(\frac{\sum_{m=0}^{5}\sum_{n=0}^{2}\zeta_i^m\zeta_j^n\hat{\psi}_{1,mn}(\omega_i,\omega_j)}{D_1}\right) + \omega_j\ln(\omega_j)\left(\frac{\sum_{m=0}^{5}\sum_{n=0}^{2}\zeta_i^n\zeta_j^m\hat{\psi}_{1,mn}(\omega_j,\omega_i)}{D_2}\right)\right.
\end{aligned}$$

$$+\ln\left(\nu_{\mathrm{g}}\right)\left(\frac{\sum_{m=0}^{2}\sum_{n=0}^{2}D_3\zeta_i^m\zeta_j^n\hat{\xi}_{1,mn}(\omega_i,\omega_j)+D_4\zeta_i^n\zeta_j^m\hat{\xi}_{1,mn}(\omega_j,\omega_i)}{2\zeta_{\mathrm{g}}D_3D_4}\right)\Bigg], \tag{37}$$

$$\lambda_{2,ij}=G_0\pi\omega_i\omega_j\nu_{\mathrm{g}}^2\left[\frac{\nu_{\mathrm{g}}\sum_{m=0}^{2}\sum_{n=0}^{2}\zeta_i^m\zeta_j^n\xi_{2,mn}(\omega_i,\omega_j)}{4\zeta_{\mathrm{g}}D_4}+\frac{2\omega_i^2\sum_{m=0}^{6}\sum_{n=0}^{2}\zeta_i^m\zeta_j^n\psi_{2,mn}(\omega_i,\omega_j)}{D_1}\right], \tag{38}$$

because they are the starting point for further simplifications. The functionals $\xi_{l,mn}(\omega_i,\omega_j)$, $\psi_{l,mn}(\omega_i,\omega_j)$, $\hat{\xi}_{l,mn}(\omega_i,\omega_j)$ and $\hat{\psi}_{l,mn}(\omega_j,\omega_i)$ $(l=0,1,2)$ are sorted with respect to the exponent of the damping coefficients, m and n, which allows a linearization with respect to damping. They and the further functionals D_1–D_4 present in these equations are specified in [12,13]. The lth cross-spectral moment between the ith modal acceleration and the ground acceleration, $\lambda_{l,ig}$, follows $\lambda_{l,ij}$ with the limit of ω_j to infinity,

$$\lim_{w_j\to\infty}\left(\lambda_{l,ij}\right)=\lambda_{l,ig}. \tag{39}$$

The zeroth spectral moment and the higher moments of the ground are [12,13]:

$$\lambda_{l,gg}=\begin{cases}G_0\pi\nu_{\mathrm{g}}\left(\zeta_{\mathrm{g}}+\frac{1}{4\zeta_{\mathrm{g}}}\right) & \text{if}\quad l=0\\ \infty & \text{if}\quad l=1,2,\ldots\end{cases} \tag{40}$$

References

1. Adam, C., Furtmüller, T., Moschen, L.: Floor response spectra for moderately heavy nonstructural elements attached to ductile frame structures. In: Papadrakakis, M., Fragiadakis, M., Plevris, V. (eds.) Computational Methods in Earthquake Engineering, Computational Methods in Applied Sciences, pp. 69–89. Springer, Dordrecht (2013)
2. ASCE/SEI 7-10: Minimum design loads for buildings and other structures. American Society of Civil Engineers, Reston (2013)
3. Chopra, A.K.: Dynamics of Structures: Theory and Applications to Earthquake Engineering. Prentice Hall, Boston (2012)
4. Der Kiureghian, A.: A response spectrum method for random vibrations. UCB/EERC Report 80/15 (1980)
5. Der Kiureghian, A.: Structural response to stationary excitation. J. Eng. Mech. Div. **106**, 1195–1213 (1980)
6. Der Kiureghian, A.: A response spectrum method for random vibration analysis of MDF systems. Earthq. Eng. Struct. Dyn. **9**, 419–435 (1981)
7. Der Kiureghian, A., Nakamura, Y.: CQC modal combination rule for high-frequency modes. Earthq. Eng. Struct. Dyn. **22**, 943–956 (1993)
8. FEMA E-74: Reducing the risks of nonstructural earthquake damage—a practical guide. (2012)
9. Filiatrault, A., Sullivan, T.: Performance-based seismic design of nonstructural building components: the next frontier of earthquake engineering. Earthq. Eng. Eng. Vib. **13**(1), 17–46 (2014)
10. Heredia-Zavoni, E.: The complete SRSS modal combination rule. Earthq. Eng. Struct. Dyn. **40**, 1181–1196 (2011)
11. Kanai, K.: Semi-empirical formula for the seismic characteristics of the ground. Bull. Earthq. Res. Inst. **35**, 309–325 (1957)
12. Moschen, L.: Contributions to the Probabilistic Seismic Assessment of Acceleration Demands in Buildings. Ph.D. Thesis, University of Innsbruck, Innsbruck Austria (2016)
13. Moschen, L., Adam, C., Vamvatsikos, D.: A response spectrum method for peak floor acceleration demands in earthquake excited structures. J. Prob. Eng. Mech. **46**, 94–106 (2016)
14. Moschen, L., Medina, R.A., Adam, C.: A ground motion record selection approach based on multi-objective optimization (2016) (to be submitted)
15. Pacific Earthquake Engineering Research Center: PEER ground motion database. University of California, Berkeley (2010)
16. Pozzi, M., Der Kiureghian, A.: Response spectrum analysis for floor acceleration. In: Proceedings of the 15th World Conference on Earthquake Engineering (15WCEE). Lisbon (2012)
17. Pozzi, M., Der Kiureghian, A.: Response spectrum analysis for floor acceleration. Earthq. Eng. Struct. Dyn. **44**, 2111–2127 (2015)
18. Rice, S.O.: Mathematical analysis of random noise. Bell Syst. Tech. J. **3**, 282–332 (1944)
19. Rosenblueth, E.: A Basis for Aseismic Design. Ph.D. Thesis, University of Illinois, Urbana (1951)
20. Shome, N., Cornell, C.A., Bazzurro, P., Carballo, J.E.: Earthquakes, records and nonlinear MDOF responses: RMS report no. 29. Reliability of Marine Structures Program, Department of Civil Engineering, Stanford University (1997)
21. Shome, N., Cornell, C.A., Bazzurro, P., Carballo, J.E.: Earthquakes, records, and nonlinear responses. Earthq. Spectra **3**, 469–500 (1998)
22. Sullivan, T., Calvi, P., Nascimbene, R.: Towards improved floor spectra estimates for seismic design. Earthq. Struct. **4**(1), 109–132 (2013)
23. Taghavi, S.: Probabilistic Seismic Assessment of Floor Acceleration Demands in Multi-story Buildings. Ph.D. Thesis, Stanford University (2006)
24. Taghavi, S., Miranda, E.: Response spectrum method for estimation of peak floor acceleration demand. In: Proceedings of the 14th World Conference on Earthquake Engineering (14WCEE). Beijing (2008)

25. Taghavi, S., Miranda, E.: Response spectrum method for estimation of estimation of peak floor acceleration demands. In: B. Goodno (ed.) ATC and SEI Conference on Improving the Seismic Performance of Existing Buildings and Other Structures, pp. 627–638. San Francisco (2009)
26. Tajimi, H.: A statistical method of determining the maximum response of a building structure during an earthquake. In: Proceedings of the 2nd World Conference on Earthquake Engineering (2WCEE), pp. 781–797. Tokyo and Kyoto (1960)
27. Vanmarcke, E.H.: Properties of spectral moments with appilcations to random vibration. J. Eng. Mech. Div. **98**, 425–446 (1972)
28. Vanmarcke, E.H.: On the distribution of the first-passage time for normal stationary random processes. J. Appl. Mech. **42**, 215–220 (1975)
29. Vukobratović, V., Fajfar, P.: A method for the direct determination of approximate floor response spectra for SDOF inelastic structures. Bull. Earthq. Eng. **5**, 1405–1424 (2015)